

## Two-electron reaction in nanoporous cathode material for Lithium ion secondary battery

Tomoyuki Matsuda<sup>1</sup> and Yutaka Moritomo<sup>1,2</sup>

<sup>1</sup>Graduated School of Pure and Applied Science, University of Tsukuba, Tsukuba 305-8571, Japan  
<sup>2</sup>TIMS, University of Tsukuba, Tsukuba305-8571, Japan

### 1 Introduction

Lithium ion batteries have aided the portable electronics revolution during the past two decades, and are now being intensively pursued for transportation applications and the efficient storage and utilization of intermittent renewable energies like solar and wind. Therefore, next-generation electrode materials have been intensively explored in order to achieve a highly-capacious, safe, environmentally-friendly, and low cost Li-ion secondary battery.

Prussian blue analogues, represented as  $A_xM[M'(CN)_6]_y \cdot zH_2O$  ( $A$  is an alkali metal ion, and  $M$  and  $M'$  are transition metal ions), have nanoporous three-dimensional network structures. Recently, we realized a good cyclability with a high charge capacity in the film-type electrode of  $Li_xMn[Fe(CN)_6]_{0.83} \cdot 3.5H_2O$  [1,2]. The film-type electrode does not contain a conductive material nor a binder polymer. Here, we present structure and valence states of  $Li_xMn[Fe(CN)_6]_{0.83} \cdot 3.5H_2O$  against Li concentration ( $x$ ). The data clearly indicates that the compound exhibits two-electron reaction without structural phase transition.[3]

### 2 Experiment

Thin film of  $Na_{1.32}Mn[Fe(CN)_6]_{0.83} \cdot 3.5H_2O$  was electrochemically synthesized on an indium tin oxide (ITO) transparent electrode under potentiostatic conditions at  $-0.50$  V vs a standard Ag/AgCl electrode in an aqueous solution containing  $1.0 \text{ mmol dm}^{-3}$   $K_3[Fe(CN)_6]$ ,  $1.5 \text{ mmol dm}^{-3}$   $MnCl_2 \cdot 6H_2O$ , and  $1.0 \text{ mol dm}^{-3}$  NaCl. The obtained film was transparent with a thickness of around  $1 \mu\text{m}$ . Chemical compositions of the films were determined by the inductively coupled plasma (ICP) method and CHN organic elementary analysis (Perkin-Elmer 2400 CHN Elemental Analyzer). The  $Li^+$  was substituted for  $Na^+$  by performing the charge/discharge cycles of the thin film against Li. Thus, we obtained thin films of  $Li_xMn[Fe(CN)_6]_{0.83} \cdot 3.5H_2O$ . The thin film was used as prepared (film-type electrode). The lithium metal was used as the reference and counter electrode, and the cut-off voltage was from 2.0 to 4.3 V. The electrolyte was ethylene carbonate (EC) / diethyl carbonate (DEC) solution containing  $1 \text{ mol dm}^{-1}$   $LiClO_4$ .

The valence states of the Fe and Mn sites were determined by the *ex-situ* X-ray absorption spectra (XAS) around the Mn and Fe K-edge. The XAS measurements were conducted at the beamline 7C of the Photon Factory, KEK. The XAS spectra were recorded by a Lytle detector in a fluorescent yield mode with a Si(111) double-crystal monochromator at 300 K. The background subtraction and normalization were done using ATHENA program[4].

The *ex-situ* powder X-ray diffraction (XRD) patterns were measured at the beamline 8A of KEK-PF equipped with an imaging plate detector. The charged/discharged samples were washed with DEC, and were carefully removed from the ITO glasses. The obtained powders were sealed in  $300 \mu\text{m}$  glass capillaries. XRD patterns were measured at 300 K and the exposure time was 5 min. Wavelength of the X-ray was  $0.77516 \text{ \AA}$ . The lattice constants of each compound were refined by the RIETAN-FP program [5].

### 3 Results and Discussion

Figure 1 shows the charge/discharge curve of the film-type electrode of  $Li_{1.32}Mn[Fe(CN)_6]_{0.83} \cdot 3.5H_2O$  at the 2nd cycle. We electrochemically controlled the Li ion concentration ( $x$ ) as indicated by the arrows.

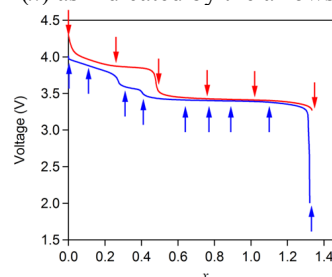


Fig. 1: Voltage vs composition curves for charge (red) and discharge (blue) process of film-type electrode of  $Li_xMn[Fe(CN)_6]_{0.83} \cdot 3.5H_2O$  thin film at the 2nd cycle. The arrows indicate the compositions for the XAS and XRD measurements.

Figure 2a shows the Fe K-edge XAS spectra of charge/discharge process. The absorption peak energies ( $E$ ) in the Fe K-edge spectra show clear blue shift with

decrease in  $x$  (Figure 2b). The blue shift is ascribed to the oxidation of Fe (low spin  $\text{Fe}^{\text{II}} \rightarrow$  low-spin  $\text{Fe}^{\text{III}}$ ). We emphasize that the blue shift saturates below  $x = 0.46$  (0.41) in the charging (discharging) process. Figure 3a shows the Mn K-edge XAS spectra of charge/discharge process. The shoulder peak appeared around 6553 eV in the small- $x$  region. This new peak is ascribed to the oxidation of Mn (high spin  $\text{Mn}^{\text{II}} \rightarrow$  high-spin  $\text{Mn}^{\text{III}}$ ) [10]. These data indicated that the oxidation of Fe takes place in the large- $x$  region, while the oxidation of Mn takes place in the small- $x$  region.

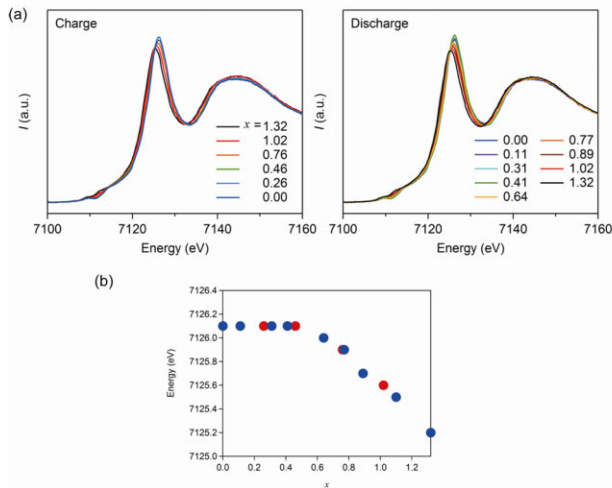


Fig. 2: (a) Fe K-edge XAS spectra for the charging (left), discharging (right) processes of film-type electrode of  $\text{Li}_x\text{Mn}[\text{Fe}(\text{CN})_6]_{0.83}\cdot 3.5\text{H}_2\text{O}$ . (b) Peak energy ( $E(x)$ ) against  $x$  for the charging (red) and discharging (blue) processes.

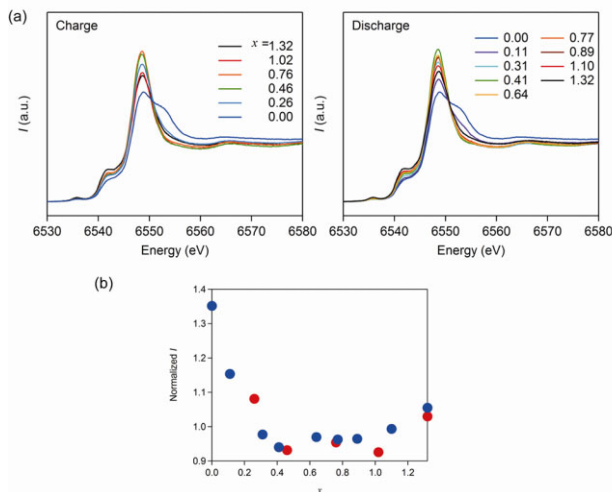


Fig. 3: (a) Mn K-edge XAS spectra for the charging (left), discharging (right) processes of film-type electrode of  $\text{Li}_x\text{Mn}[\text{Fe}(\text{CN})_6]_{0.83}\cdot 3.5\text{H}_2\text{O}$ . (b) Normalized intensity ( $I(x)$ ) against  $x$  for the charging (red) and discharging (blue) processes.

Figure 4 shows the magnified XRD patterns during charge/discharge process. The lattice structure remains the face-centered cubic ( $Fm\bar{3}m$ ;  $Z = 4$ ) throughout the charge/discharge process. In the charging process, the

reflection shifts to the lower-angle side above  $x = 0.76$  while shifts to the lower-angle side below  $x = 0.46$ . In the discharging process, the reflection shifts to the lower-angle side below  $x = 0.41$  while shifts to the higher-angle side above  $x = 0.64$ .

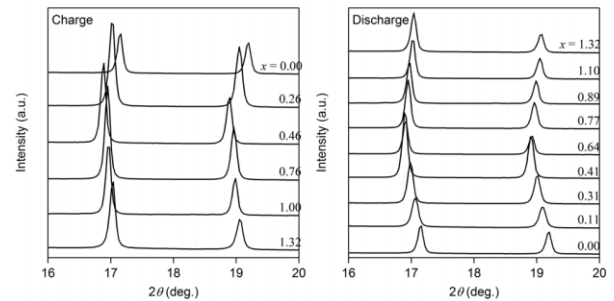


Fig. 4: XRD patterns for the charging (left) and discharging (right) processes of film-type electrode of  $\text{Li}_x\text{Mn}[\text{Fe}(\text{CN})_6]_{0.83}\cdot 3.5\text{H}_2\text{O}$ .

Figures 5a and 5b show the molar ratios of the  $\text{Fe}^{\text{III}}$  and  $\text{Mn}^{\text{III}}$  against  $x$ , respectively. These data clearly indicate the charge/discharge process of the film-type electrode consists of the two reactions, i.e.,  $\text{Mn}^{\text{II}}/\text{Mn}^{\text{III}}$  and  $\text{Fe}^{\text{II}}/\text{Fe}^{\text{III}}$  reactions. The  $\text{Mn}^{\text{II}}/\text{Mn}^{\text{III}}$  reaction takes place in the small- $x$  region ( $x < 0.46$ : indicated by vertical broken line in Fig.5), while the  $\text{Fe}^{\text{II}}/\text{Fe}^{\text{III}}$  reaction takes place in the large- $x$  region ( $x > 0.46$ ). The first and second plateaus in the charging process (see Fig.1) are ascribed to the oxidation of  $\text{Mn}^{\text{II}}$  and  $[\text{Fe}^{\text{II}}(\text{CN})_6]^{4-}$ , respectively. On the contrary, the first, second and third plateaus in the discharge process is due to the reduction of  $\text{Mn}^{\text{III}}$ ,  $\text{Mn}^{\text{II}}$ , and  $[\text{Fe}^{\text{III}}(\text{CN})_6]^{3-}$ , respectively.

Figure 5c shows the lattice constant against  $x$ . The lattice constants were refined by the Rietveld analysis. In the  $\text{Mn}^{\text{II}}/\text{Mn}^{\text{III}}$  redox region, the lattice constant increases with  $x$ . The increase is ascribed to the larger ionic radius of  $\text{Mn}^{\text{II}}$ . In the  $\text{Fe}^{\text{II}}/\text{Fe}^{\text{III}}$  region, the lattice constant decreases with  $x$ . The decrease is ascribed to the smaller size of  $[\text{Fe}^{\text{II}}(\text{CN})_6]^{4-}$  as compared with that of  $[\text{Fe}^{\text{III}}(\text{CN})_6]^{3-}$ .

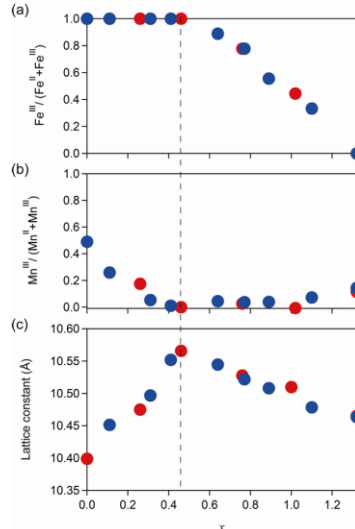


Fig. 4: (a) Molar ratios of the Fe<sup>III</sup>, (b) molar ratios of the Mn<sup>III</sup> (b), and (c) lattice constants for the charging (red) and discharging (blue) processes of Li<sub>x</sub>Mn[Fe(CN)<sub>6</sub>]<sub>0.83</sub>·3.5H<sub>2</sub>O.

#### Acknowledgement

This work was supported by a Grant-in-Aid (21244052) for Scientific Research from the Ministry of Education, Culture, Sports, Science and Technology. Elementary analysis was performed at Chemical Analysis Division, Research Facility Center for Science and Engineering, University of Tsukuba. The X-ray powder diffraction and X-ray absorption experiments were performed under the approval of the Photon Factory Program Advisory Committee (Proposal No. 2010G502 and 2011G501).

#### References

- [1] T. Matsuda, and Y. Moritomo, *Appl. Phys. Express*, **4** (2012) 047101.
- [2] Y. Moritomo, M. Takachi, Y. Kurihara, and T. Matsuda, *Appl. Phys. Express*, **5** (2012) 041801.
- [3] T. Matuda and Y. Moritomo, *J. Nanotech*, (2012) 568147.
- [4] B. Ravel, and M. Newville, *J. Synchrotron Radiation*, **12** (2005) 537-541.
- [5] F. Izumi, and K. Momma, *Solid State Phenomena*, **130** (2007) 15-20.

\* pf-acr2011@kek.jp